IEEE Access
Multidisciplinary | Rapid Review | Open Access Journal

Received November 2, 2018, accepted November 29, 2018, date of publication December 11, 2018,
date of current version October 22, 2019

Digital Object Identifier 10.1109/ACCESS.2018.2885709

Supraspinatus Segmentation From Shoulder Ultrasound Images Using a Multilayer Self-Shrinking Snake

YOU-WEI WANG[1,2], CHUNG-CHIEN LEE[3,4,5], AND CHUNG-MING LO[2,6]

[1]Department of Computer Science and Information Engineering, National Taiwan University, Taipei 106, Taiwan
[2]College of Medical Science and Technology, Graduate Institute of Biomedical Informatics, Taipei Medical University, Taipei 106, Taiwan
[3]Graduate Institute of Biomedical Electronics and Bioinformatics, National Taiwan University, Taipei 106, Taiwan
[4]Department of Orthopedic Surgery, New Taipei City Hospital, New Taipei City 241, Taiwan
[5]Department of Orthopedic Surgery, National Taiwan University Hospital, Taipei 100, Taiwan
[6]Graduate Institute of Library, Information and Archival Studies, National Chengchi University, Taipei 116, Taiwan

Corresponding author: Chung-Ming Lo (buddylo@tmu.edu.tw)

This work was supported in part by the Ministry of Science and Technology under Grant MOST 106-2221-E-038-018 and Grant MOST 107-2221-E-038-017, and in part by New Taipei City Hospital of the Republic of China under Grant NTCH104-001.

ABSTRACT Over people's lifetimes, the prevalence of shoulder pain exceeds 70%. In particular, 70% of shoulder pain is caused by the rotator cuff lesions that are located in the supraspinatus area. The automatic and quantitative segmentation of the supraspinatus area can provide a more-objective and accurate assessment of the rotator cuff lesions. In this paper, 108 shoulder ultrasound images comprised the image database to evaluate the proposed segmentation method, and a multilayer self-shrinking snake (S^3), based on a multilayer segmentation framework, was used to achieve optimal segmentation. Using a rough initial contour that enclosed the supraspinatus area, the modified snake was shrunken with an iteration procedure according to the boundary conditions that included the elasticity, curvature, gradient, and distance. In the performance evaluation, S^3 achieved an F-measure of 0.85. The success of S^3 could provide more-objective location information to physicians diagnosing rotator cuff lesions.

INDEX TERMS Ultrasound, shoulder pain, rotator cuff, segmentation, supraspinatus segmentation, snake.

I. INTRODUCTION

The lifetime prevalence of shoulder complaints is 70% [1]. Shoulder pain may lead to an inability to work and carry out activities of daily living, which is a burden to both patients and society. Each year, health authorities in the United States spend $7 billion for shoulder pain, which is also responsible for 13% of sick leave [2]. Among the causes of shoulder pain, rotator cuff lesions account for up to 70% [3], [4]. Neer's classification summarizes rotator cuff lesions into three phases [5]: inflammatory responses (localized swelling and bleeding), calcification and fibrosis, and full- or partial-thickness tears.

Populations suffering from rotator cuff lesions have shoulder pain and difficulties gripping due to limited forward elevation, and weak abduction and external rotation. Tears, the most-severe lesions, have a prevalence rate of 20.7% and worsen previous limitations. The prevalence rate of tears is expected to increase due to the current aging of societies worldwide.

Clinically, the severity of rotator cuff lesions affects the effectiveness of commonly used clinical tests, and physical examinations are considered unreliable in diagnosing rotator cuff lesions [6]. Also, inter-observer variabilities exist between physicians, which makes it difficult to reach a consensus [7]. A proper assessment relies on imaging modalities such as ultrasound (US), but magnetic resonance imaging (MRI) is more practical [8]. Shoulder US was suggested to be an effective tool for detecting rotator cuff lesions [9]–[11] and full-thickness tears. The performance achieved by experienced musculoskeletal radiologists or shoulder orthopedic surgeons is comparable to that with MRI [11], [12]. However, lower accuracy is likely obtained when diagnosed by general radiologists or US technicians [13]. Inter-operator variability should be reduced to strengthen the role of US in clinical use.

The difficulties of the supraspinatus segmentation due to the low contrast and speckle noises in the US images which lead to unobvious boundary and incomplete region of target.

Suppressing the effect caused by speckle noises is critical to obtain complete supraspinatus boundaries. In recent studies, Gupta *et al.* [14] proposed an approach to determine the orientation of the supraspinatus area in US images by curvelet transformation. The curvelet transformation approximated the shape of supraspinatus area with a roughly smooth curve. Jabbar *et al.* [15] used a convolutional neural network (CNN) to segment supraspinatus areas. CNN relies on definite labeling to do supervised learning but the boundaries of supraspinatus areas in US are blurred. The high uncertainty may affect the segmentation accuracy. The result can be compared to the study of Kim *et al.* [16] which used MRI for automatic supraspinatus segmentation. With high resolution and less noises, MRI segmentation achieved better results. To make US become more promising in clinical use, the challenging of supraspinatus segmentation in US should be addressed.

Quantitative analyses are increasingly needed to provide objective accordance to reduce variability among operators. Thus, this study proposes a quantitative method for supraspinatus segmentation from shoulder US images. Fig. 1 illustrates that numerous line segments can appear in rotator cuff lesions in original shoulder US images.

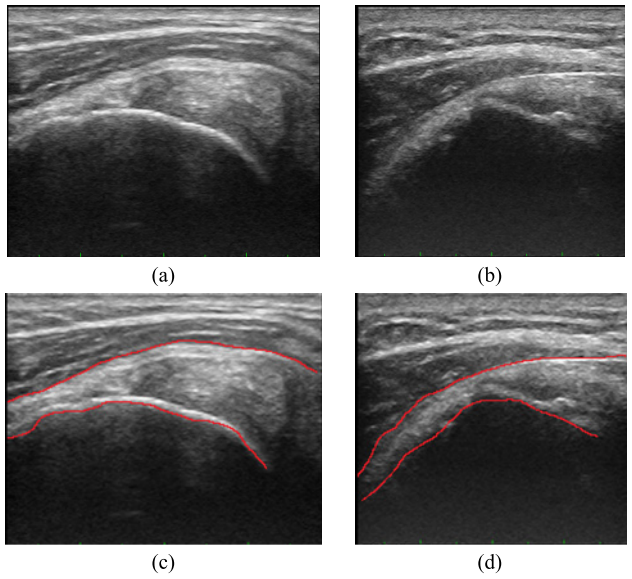

FIGURE 1. **Supraspinatus areas shown on shoulder ultrasound. The red lines in (c) and (d) are manually delineated boundaries of supraspinatus areas in (a) and (b), respectively.**

Manually delineating supraspinatus areas is time consuming and induces substantial inter- and intra-operator variability. To obtain a balance between accuracy and efficiency, a semiautomatic supraspinatus segmentation procedure using a multilayer self-shrinking snake (S^3) was developed. In comparison, the level-set method is commonly used in tumor segmentation [17]. However, there are numerous positions for defining seeds, by users, which can lead to operator-dependence. Another issue is that a growing contour from positions inside the target area may cause leakage at the unclear boundary close to the background. The proposed S^3 uses an objective region of interest (ROI) as an initial contour that is then shrunken to the target area, thereby avoiding this problem. When using the S^3, anatomical structures on shoulder US images need to be further clarified. Analyzing tissues enclosed in the segmented area can provide more-reliable diagnostic information for physicians.

II. MATERIALS AND METHODS

A. US ACQUISITION

This study was approved by the institutional review board of New Taipei City Hospital (New Taipei City, Taiwan), and informed consent was waived because it was a retrospective study. In total, 108 shoulder US images were obtained from January 2011 to February 2014. An Aloka alpha-6 US scanner (Hitachi-Aloka Medical, Tokyo, Japan) with a linear array probe (width: 36 mm) ranging 5∼13 MHz was used for the examination. Scanner settings were consistent for all patients. A standard sitting position and a routine procedure were followed. The acquired images were transformed from Digital Imaging and Communications in Medicine to BMP format and stored as 8-bit files that ranged 0∼255. A shoulder orthopedic surgeon was in charge of delineating the supraspinatus areas as the gold standard to evaluate the segmentation method.

B. MULTILAYER S^3

The main idea of the proposed segmentation method, the S^3, is a modified form of a snake [18]–[20] with an initial contour defined as a bounding box to enclose the supraspinatus area. As it evolves, the initial contour automatically shrinks to the desired boundary in multiple layers of iterations. As shown in Fig. 2, the flowchart of the S^3 illustrates the serial steps and corresponding middle images.

S^3 is a multi-layer self-shrinking iteration that combines noise reduction, shape description, and classification techniques to establish an architecture to deal with the inherent noisy appearance of US images. To our knowledge, this is the first study to systematically deal with speckle noise. For contour convergence, a newly developed distance force is combined with the other three conventional forces, i.e., the elasticity, curvature, and gradient, to fit the edges. The distance force is especially useful for determining whether an edge gradient exists between the speckle noise and background tissues.

After preprocessing for noise suppression, the first layer using a Hough transformation [21] followed by the S^3 was performed to obtain dominant boundaries inside the initial contour. The Hough transformation extracts meaningful line segments according to characteristics of the supraspinatus boundaries, such as the angle and lengths of horizontal and vertical lines. The next layers further optimize the boundaries using Otsu's method [22] and the S^3. Otsu's method considers the echogenic composition inside the detected boundaries which can become a useful criterion, since the supraspinatus

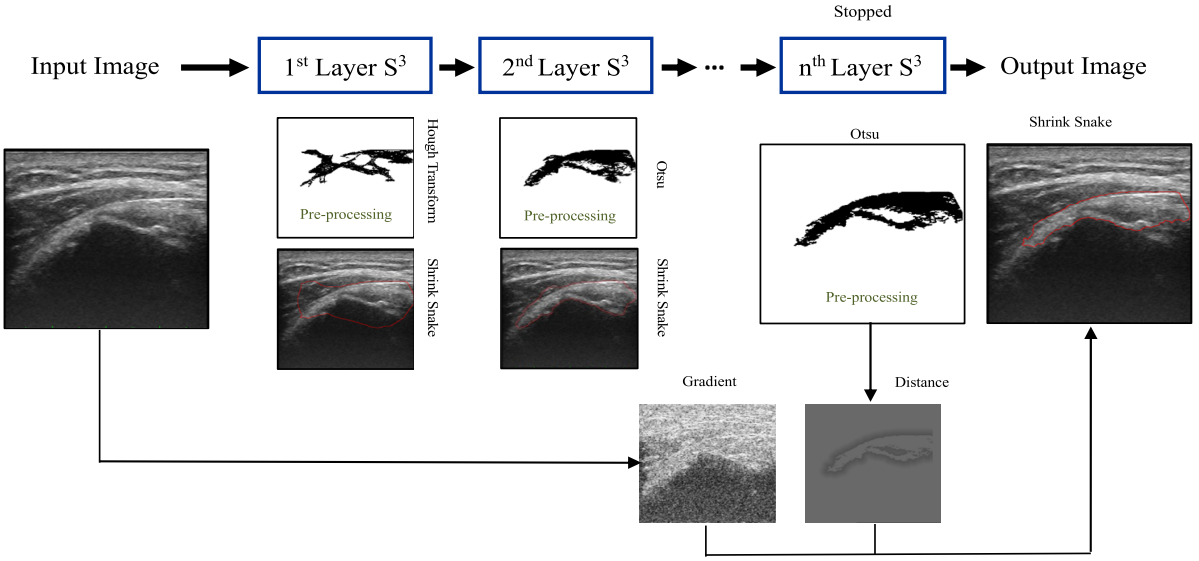

FIGURE 2. The automatic segmentation rotator cuff framework.

area has a clear edge between internal hyperechogenic tissues and external hypoechogenic tissues. The S^3, the core of boundary detection, was formulated using the elasticity, curvature, gradient, and distance.

C. PRE-PROCESSING

Speckle noise inherent in US images has a granular appearance with intensity variations in gray levels. Suppressing the effect caused by speckle noise is critical to obtain complete supraspinatus boundaries. While conventional noise-removing filters, including mean and median filters, can locally reduce the noise, the boundaries are more or less simultaneously blurred. In the experiment, anisotropic diffusion [23] was used to improve the image quality while preserving important boundary information (Fig. 3b). The formula is listed below:

$$\frac{\partial}{\partial t} I(x, y, t) = div\left[c\left(\|\nabla I\|\right) \cdot \nabla I\right]; \tag{1}$$

where *div* indicates a divergence function for the gradient operator ∇, and $||\cdot||$ is the magnitude. $I(x,y,0)$ is the initial image with x and y as coordinates, and t is the iteration step. $c(||\nabla I||)$ is the diffusion function that monotonically decreases by means of the gradient magnitude.

D. MULTILAYER OPTIMIZATION

As previously mentioned, segmentation was optimized using a multilayer approach. The first layer was composed of a Hough transformation [21] and the S^3. The Hough transformation is powerful in detecting straight lines to preserve the characteristic and structural information of the supraspinatus. In our observations, supraspinatus boundaries had longer horizontal and shorter vertical line segments which became target lines in the Hough transformation. Using the definition below, the original US image was transformed into a domain

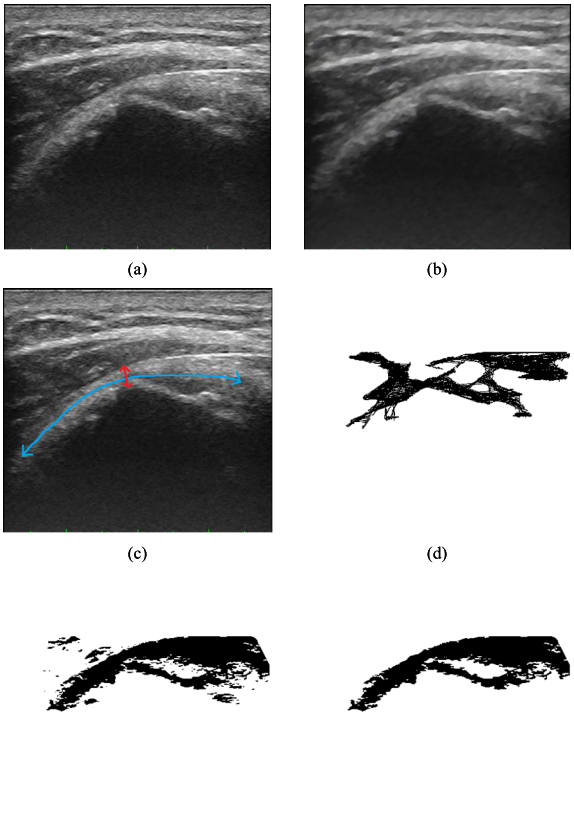

FIGURE 3. An example of the segmentation procedure. (a) The original ultrasound image. (b) After anisotropic diffusion smoothing. (c) Line characteristics of the rotator cuff boundary. (d) The Hough transformation result after Otsu's binarization. (e) Supraspinatus area extraction according to echogenicity. (f) The remaining maximum region fed to the next layer.

of line segments with different angles:

$$I(x, y) \Rightarrow R = x\cos(\theta) + y\sin(\theta). \tag{2}$$

The lines of interest (Fig. 3c) were within the defined angle range of $-60°$ to $60°$, the lengths exceeded 40 pixels, and the

gap was 40 pixels between lines. In the first layer, rough but satisfactory initial boundaries were obtained. Taking n as the total number of iterations, the other n-1th layers composing Otsu's method [22] and the S^3 were continuously applied to fine-tune the boundaries. Otsu's method can automatically separate echogenicities of tissues enclosed by the boundaries into two groups as follows:

$$\mu_a = \frac{\sum_{i=0}^{t} h(i) \times i}{\sum_{i=0}^{t} h(i)}, \tag{3}$$

$$\mu_b = \frac{\sum_{i=t+1}^{255} h(i) \times i}{\sum_{i=t+1}^{255} h(i)}, \tag{4}$$

$$\sigma_a(t) = \sum_{i=0}^{t} (\mu_a - i)^2 \times h(i), \tag{5}$$

$$\sigma_b(t) = \sum_{i=t+1}^{255} (\mu_b - i)^2 \times h(i), \quad \text{and} \tag{6}$$

$$T = \arg\min_t (\sigma_a(t) + \sigma_b(t)); \tag{7}$$

where $h(i)$ is the number of intensity i, and T is the threshold of Otsu's method. Tissues were separated into two groups, a and b, according to their echogenicities.

Due to the fact that there was a clear edge between internal hyperechogenic tissues and external hypoechogenic tissues in the supraspinatus area, the result in Fig. 3e can be obtained. Leaving the dominant region while removing surrounding noise, Fig. 3f shows another initial but more-accurate boundary to the subsequent S^3. Iterations were continuously executed until the difference between the nth and n-1th layers was < 20 pixels.

E. SELF-SHRINKING SNAKE (S^3)

The S^3 performed in each layer is the fundamental basis of the proposed segmentation method. It is a modified form of a snake guided by constraint terms and target information using control points on the initial boundary that are shrunken to the target supraspinatus. During the evolution, how the S^3 shrinks depends on the balance of four forces: the elasticity, curvature, gradient, and distance. Combining the four forces together determines the linked edges between control points on the evolving boundary to achieve the S^3:

For all N pixels, p_i, in the initial ROI, p is the set of control points, where $i = 1 \ldots N$, and N depends on the size of the initial ROI.

$$S^3(p_i) = \arg\min_v (Ela + Cur + Gra + Dist), \quad v \subset neighbors\ of\ p_i \tag{8}$$

In Eq. (8), each control point, p_i, finds the minimum of the energy function, S^3, to move the control point, p_i, to the new position, and the decision rule is according to the neighbors of p_i at v: $\{(x-1, y-1), (x, y-1), (x+1, y-1), (x-1, y), (x+1, y), (x-1, y+1), (x, y+1), (x+1, y+1)\}$ by a 3×3 mask, which has the minimum energy of S^3. v is the set of candidate pixels in the mask which p is moving to. Same definition of v is in Eq. (10), (11), (13) and (14).

- *Elasticity*:

$$\bar{d} = \frac{\|p_N - p_1\| + \sum_{j=1}^{N-1} \|p_{j+1} - p_j\|}{N}, \tag{9}$$

$$Ela = \left|\bar{d} - \|v - p_{i-1}\|\right|, \tag{10}$$

- *Curvature*:

$$Cur = \|(p_{i+1} - v) + (p_{i-1} - v)\|^2, \tag{11}$$

- *Gradient*:

$$g(x, y) = \sqrt{(I(x+1, y) - I(x, y))^2 + (I(x, y+1) - I(x, y))^2}, \tag{12}$$

$$Gra = \max\_gradient - g(v(x, y)), \tag{13}$$

and

- *Distance*:

$$Dist = Closest(\|v - Target\|); \tag{14}$$

where elasticity defines the gap between all of the control points that can be used to restrict the contour shrinkage. $\bar{d}$ is the average distance between pairs of p in each iteration. Curvature limits the bending conditions of the curve. For example, a larger value indicates a curvier line, and a smaller value indicates an approximate straight line. Gradient is the difference between function g and the maximum gradient in the image denoted by *max_gradient* in Eq. (13); g is the difference between adjacent pixels in both the horizontal and vertical directions. High gray-scale variations around the boundary result in high gradients. A newly developed distance force was proposed for the energy function. Distance is the shortest distance between the control points and the target region. The distance force is especially useful for determining whether the edge gradient exists between speckle noise and background tissues, and the output region of each layer after the Hough or Otsu method denoted by *Target* in Eq. (14). In equations (9∼14), parameter p is the control point set, and N is the number of control points, so p_i is index i of control point p. I (x, y) means the intensity value of the coordinate x and y on the image. However, control point p_i also has information on coordinates x and y, and similarly is related to I (x, y). A control point is moved to the next position which has the minimum argument of the four forces in the eight connected neighbors (a 3×3 mask). A flowchart of S^3 is shown in Fig. 4. If two control points are too close to each other, these two are replaced by a single new control point between them. On the other hand,

a new control point is inserted between two distant points. This manipulation takes both efficiency and smoothness into consideration.

We followed the modified snake, i.e., the greedy algorithm by Williams and Shah, rather than the original snake, i.e., Snake: Active Contour Model of Kass *et al.* [18] and Williams and Shah [19], [20]. The difference is that the greedy algorithm makes locally minimum optimal choices, and the final solution is the globally optimal result for the target contour. In our multilayer process, each iteration determines the minimum sum of the four forces including *Ela*, *Cur*, *Gra*, and *Dist* in Eq. (8) to optimize boundary detection. The iteration in Fig. 4 is a necessary procedure used to suppress speckle noise in US images. Speckle noise appears as extremely high or low intensities in the range of 0∼255 in US images. Differentiating the difference of the true boundary and speckle noise is not deterministic and should be refined in the iteration for accuracy.

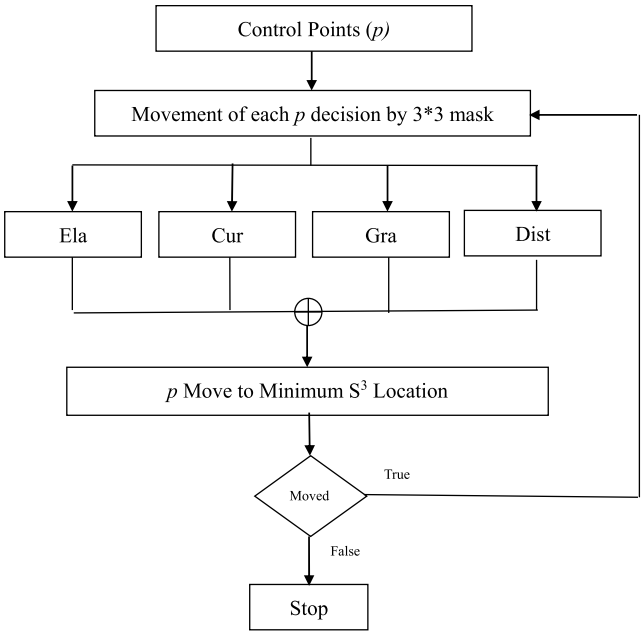

FIGURE 4. Flowchart of the self-shrinking snake (S^3).

III. EXPERIMENTAL RESULTS

In total, 108 shoulder US images were used to evaluate the proposed segmentation method. Taking the manual delineation of an orthopedist as the gold standard, the performance of the S^3 was verified. The accuracy, precision, recall, and F-measure were the performance metrics used in the evaluation. 'Accuracy' estimates how much area was detected without involving unnecessary background tissues. 'Precision' is also called the positive predictive value, and 'recall' is the sensitivity measuring the relevance. The 'F-measure' can be used to represent the relationship between precision and recall. Definitions of these performance metrics are as follows:

$$\text{Accuracy} = \frac{S^3 \cap STD}{S^3 \cup STD}, \tag{15}$$

$$\text{Precision} = \frac{TP}{TP + FP}, \tag{16}$$

$$\text{Recall} = \frac{TP}{TP + FN}, \quad \textit{and} \tag{17}$$

$$\text{F-measure} = \frac{2 \times (\textit{precision} \times \textit{recall})}{\textit{precision} + \textit{recall}}; \tag{18}$$

TABLE 1. Statistics of performance indices for supraspinatus segmentation.

	Min.	First quartile	Median value	Third quartile	Max.
Accuracy	0.26	0.60	0.70	0.75	0.86
Precision	0.49	0.75	0.88	0.95	1.00
Recall	0.29	0.71	0.79	0.87	1.00
F-measure	0.41	0.75	0.82	0.86	0.92

where S^3 is the segmentation result, and *STD* (standard) is the gold standard. TABLE 1 shows distributions of the performance indices. Fig. 5 shows two examples with successful segmentation results and box plots of four performance indices. On average, the accuracy, recall, precision, and F-measure were respectively 0.75, 0.89, 0.83, and 0.85. The proposed method could advantageously handle images with noise. Taking the results in

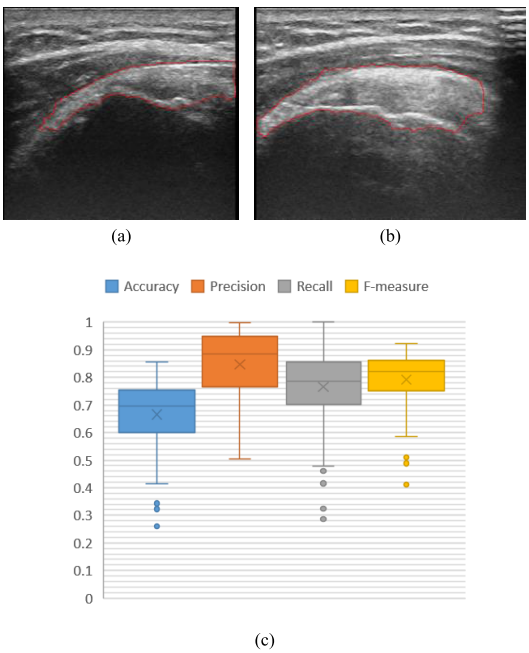

FIGURE 5. Two examples (a and b) with successful segmentation results and box plots (c) of four performance indices.

Fig. 6 as an example, the multilayer $S^3$was noise resistant. F-measure values of the two examples in

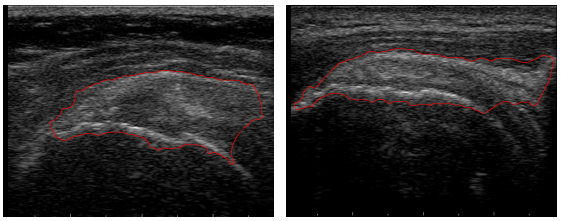

FIGURE 6. Two supraspinatus ultrasound images with substantial noise that were successfully segmented.

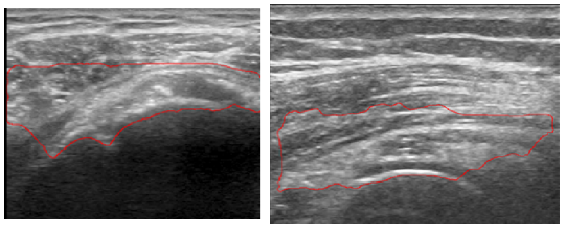

FIGURE 7. Two ultrasound images with unsatisfactory segmentation and low contrast.

Fig. 6 were 0.86 and 0.92, respectively.This advantage is especially useful in segmenting regions in US images.

Fig. 7 shows two low-contrast examples, which would normally lead to failure of accurate segmentation.

IV. DISCUSSION

This study proposed a multilayer shrinking snake procedure, the multilayer S^3, to segment the supraspinatus on shoulder US images. A simple bounding box enclosing the supraspinatus area was defined as the initial contour. During evolution, the initial contour was automatically shrunken to the desired boundary with multiple layers of iterations. The F-measure was used in the experiment to evaluate the performance of the proposed segmentation method [24]. The resulting F-measure at 0.85 indicated that the segmentation method was satisfactory. From Fig. 6, the $S^3$was demonstrated to be noise resistant.

In the evaluation, several commonly used segmentation methods, including level-set, fast marching, and the original snake, were compared in the experiment. Level-set is capable of segmenting medical images, but different positions of the initial seeds greatly affect the results [17] as shown in Fig. 8a. The supraspinatus area is composed of heterogeneous tissues, and it is a challenge to define initial seeds. Fast marching is similar to region growing, which evolves the seeds to the target boundaries [17] as shown in Fig. 8b. Also, different locations of the initial seeds result in inconsistent segmentation. The original snake, as shown in Fig. 8c, using the initial contour without the fine-tuning process as shown in S^3 resulted in poor segmentation. TABLE 2 shows that F-measures of the level-set, fast marching, and original snake were < 0.73, 0.36, and 0.70, respectively. These results indicate that they were not customized to resolve segmentation in noisy situations.

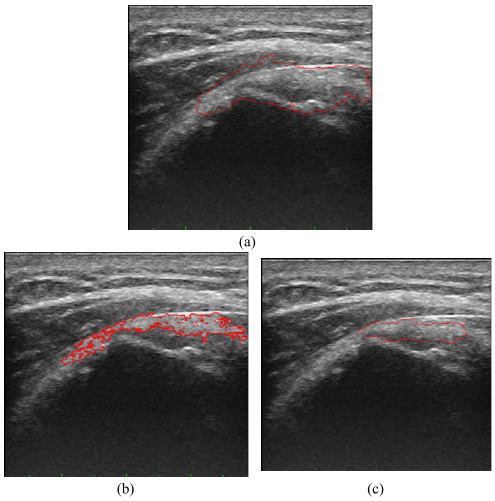

FIGURE 8. Supraspinatus segmentation results by various existing methods. (a) Level-set, (b) fast marching, and (c) the original snake.

TABLE 2. Performance comparisons of different segmentation approaches.

Supraspinatus segmentation		
Approach	F-measure	Parameter
S^3	0.84 ± 0.05	
Level set [14]	< 0.73	W_a (advection) = 2.2; W_c (curvature) = 1
Fast marching [14]	< 0.36	Dist. threshold = 0.5
Original snake [15]	< 0.70	α=1; β=1; γ=1

S^3, self-shrinking snake.

In other recent studies, Gupta *et al.* [14] proposed an approach to determine the orientation of the supraspinatus area in US images by curvelet transformation. A polynomial interpolation was also used as post-processing to smooth the boundary but more or less included background tissues. Jabbar *et al.* [15] used a convolutional neural network (CNN) to segment supraspinatus areas with a close accuracy of 80% to our result. The CNN works upon high-quality labeling in supervised learning. The inherent speckle noise in US images can lead to uncertainty in determining boundaries thereby affecting CNN segmentation, and in addition, the computation cost is substantial. For the resistance of variability, Fig. 9 shows that even when applying different initial ROI sizes to the target supraspinatus, similar segmentations can be obtained.

A limitation of the multilayer S^3 is that a semiautomatic ROI definition of the initial contour is needed. A bounding box enclosing the supraspinatus boundaries should be clearly defined by the user. If the boundary is unclear, the low contrast can also cause segmentation to fail. In a future study, more anatomical information about the supraspinatus boundaries would be helpful for fully automating the segmentation process, such as a textural analysis of the surrounding fat and bone. However, whether the extra computation would be efficient for clinical use will have to be evaluated.

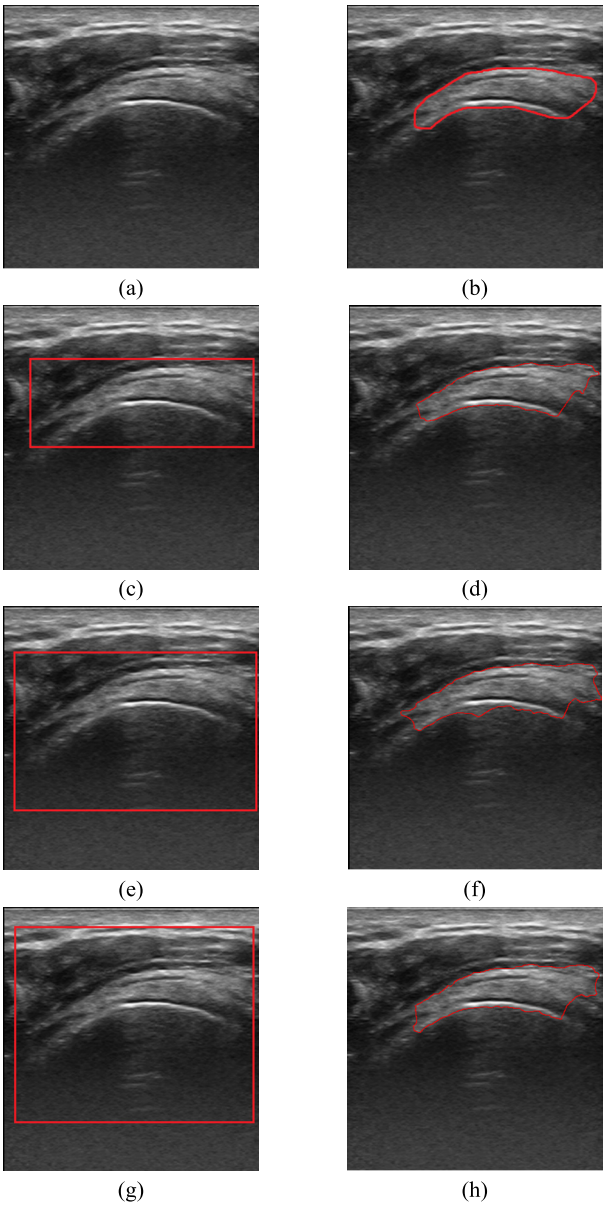

FIGURE 9. Segmentation comparisons from different initial regions of interest (ROIs). (a) Original image, (b) ground truth image; (c), (e) and (g) are initial ROIs with different sizes and positions. (d), (f), and (h) are results of (c), (e), and (g).

Other future work is to detect potential rotator cuff lesions and lesion classifications [25] in the supraspinatus region segmented by the multilayer S^3. Based on accurate segmentation, computer-aided lesion detection and diagnosis may be more useful since the location information provided by the segmented supraspinatus is more reliable. Quantitative intensity and textural features would thus be extracted to establish models with reduced variabilities.

V. CONCLUSIONS

This study proposed a S^3, a multi-layer self-shrinking iteration combining noise reduction, shape description, and classification techniques to establish an architecture to deal with the inherent noisy appearance of US images. The performance achieved an F-measure of 0.85. The accuracy can provide more-objective location information to physicians for diagnosing rotator cuff lesions.

In practice, when operating US on a patient's shoulder, general radiologists or US technicians can first define a rough area in which they are interested; then the S^3can automatically refine the detected supraspinatus area in real-time. With the rapid calculation and display on the monitor, the existence and locations of rotator cuff lesions can be better estimated. The accuracy of the diagnosis would be helpful for subsequent treatment decisions.

Potential future work would be to use the CNN to segment supraspinatus areas. Jabbar *et al.* [15] established a CNN, but it resulted in a worse performance than this study. The cause may have been speckle noise. Region-wise, rather than pixel-wise, object detection and segmentation may be another solution.

ACKNOWLEDGMENT

The publication is approved by all authors. The authors or authors' institutions have no conflicts of interest.

REFERENCES

[1] J. J. Luime *et al.*, "Prevalence and incidence of shoulder pain in the general population; a systematic review," *Scand. J. Rheumatol.*, vol. 33, no. 2, pp. 73–81, 2004.
[2] A. Hidalgo-Lozano, C. Fernández-de-las-Peñas, C. Alonso-Blanco, H.-Y. Ge, L. Arendt-Nielsen, and M. Arroyo-Morales, "Muscle trigger points and pressure pain hyperalgesia in the shoulder muscles in patients with unilateral shoulder impingement: A blinded, controlled study," *Exp. Brain Res.*, vol. 202, no. 4, pp. 915–925, 2010.
[3] G. J. Macfarlane, I. M. Hunt, and A. J. Silman, "Predictors of chronic shoulder pain: A population based prospective study," *J. Rheumatol.*, vol. 25, pp. 1612–1615, Aug. 1998.
[4] C. Mitchell, A. Adebajo, E. Hay, and A. Carr, "Shoulder pain: Diagnosis and management in primary care," *Brit. Med. J.*, vol. 331, pp. 1124–1128, Nov. 2005.
[5] C. S. Neer, "Anterior acromioplasty for the chronic impingement syndrome in the shoulder: A preliminary report," *J. Bone Joint Surg.*, vol. 54, no. 1, pp. 41–50, 1972.
[6] H. B. Park, A. Yokota, H. S. Gill, G. El Rassi, and E. G. McFarland, "Diagnostic accuracy of clinical tests for the different degrees of subacromial impingement syndrome," *J. Bone Joint Surg.*, vol. 87, no. 7, pp. 1446–1455, 2005.
[7] J. Beaudreuil *et al.*, "Contribution of clinical tests to the diagnosis of rotator cuff disease: A systematic literature review," *Joint Bone Spine*, vol. 76, pp. 15–19, Jan. 2009.
[8] R. J. Murphy, M. T. Daines, A. J. Carr, and J. L. Rees, "An independent learning method for orthopaedic surgeons performing shoulder ultrasound to identify full-thickness tears of the rotator cuff," *J. Bone Joint Surg.*, vol. 95, no. 3, pp. 266–272, 2013.
[9] G. M. Allen and D. J. Wilson, "Ultrasound of the shoulder," *Eur. J. Ultrasound*, vol. 14, no. 1, pp. 3–9, 2001.
[10] W. D. Middleton, S. A. Teefey, and K. Yamaguchi, "Sonography of the rotator cuff: Analysis of interobserver variability," *Amer. J. Roentgenol.*, vol. 183, no. 5, pp. 1465–1468, 2004.
[11] J. O. de Jesus, L. Parker, A. J. Frangos, and L. N. Nazarian, "Accuracy of MRI, MR arthrography, and ultrasound in the diagnosis of rotator cuff tears: A meta-analysis," *Amer. J. Roentgenol.*, vol. 192, no. 6, pp. 1701–1707, 2009.
[12] S. A. Teefey, D. A. Rubin, W. D. Middleton, C. F. Hildebolt, R. A. Leibold, and K. Yamaguchi, "Detection and quantification of rotator cuff tears: Comparison of ultrasonographic, magnetic resonance imaging, and arthroscopic findings in seventy-one consecutive cases," *J. Bone Joint Surg.*, vol. 86, no. 4, pp. 708–716, 2004.

[13] T. O. Smith, T. Back, A. P. Toms, and C. B. Hing, "Diagnostic accuracy of ultrasound for rotator cuff tears in adults: A systematic review and meta-analysis," *Clin. Radiol.*, vol. 66, pp. 1036–1048, Nov. 2011.
[14] R. Gupta *et al.*, "Curvelet based automatic segmentation of supraspinatus tendon from ultrasound image: A focused assistive diagnostic method," *BioMed. Eng. OnLine*, vol. 13, p. 157, Dec. 2014.
[15] S. I. Jabbar, C. R. Day, N. Heinz, and E. K. Chadwick, "Using convolutional neural network for edge detection in musculoskeletal ultrasound images," in *Proc. Int. Joint Conf. Neural Netw. (IJCNN)*, Jul. 2016, pp. 4619–4626.
[16] S. Kim, D. Lee, S. Park, K.-S. Oh, S. W. Chung, and Y. Kim, "Automatic segmentation of supraspinatus from MRI by internal shape fitting and autocorrection," *Comput. Methods Programs Biomed.*, vol. 140, pp. 165–174, Mar. 2017.
[17] J. A. Sethian, *Level Set Methods and Fast Marching Methods: Evolving Interfaces in Computational Geometry, Fluid Mechanics, Computer Vision, and Materials Science*. Cambridge, U.K.: Cambridge Univ. Press, 1999.
[18] M. Kass, A. Witkin, and D. Terzopoulos, "Snakes: Active contour models," *Int. J. Comput. Vis.*, vol. 1, no. 4, pp. 321–331, 1988.
[19] D. J. Williams and M. Shah, "A fast algorithm for active contours," in *Proc. 3rd Int. Conf. Comput. Vis.*, Dec. 1990, pp. 592–595.
[20] D. J. Williams and M. Shah, "A fast algorithm for active contours and curvature estimation," *CVGIP, Image Understand.*, vol. 55, no. 1, pp. 14–26, 1992.
[21] R. O. Duda and R. E. Hart, "Use of the Hough transformation to detect lines and curves in pictures," *Commun. ACM*, vol. 15, no. 1, pp. 11–15, Jan. 1972.
[22] N. Otsu, "A threshold selection method from gray-level histograms," *IEEE Trans. Syst., Man, Cybern.*, vol. SMC-9, no. 1, pp. 62–66, Jan. 1979.
[23] P. Perona and J. Malik, "Scale-space and edge detection using anisotropic diffusion," *IEEE Trans. Pattern Anal. Mach. Intell.*, vol. 12, no. 7, pp. 629–639, Jul. 1990.
[24] X. Zhang, X. Feng, P. Xiao, G. He, and L. Zhu, "Segmentation quality evaluation using region-based precision and recall measures for remote sensing images," *ISPRS J. Photogramm. Remote Sens.*, vol. 102, pp. 73–84, Apr. 2015.
[25] R.-F. Chang, C.-C. Lee, and C.-M. Lo, "Computer-aided diagnosis of different rotator cuff lesions using shoulder musculoskeletal ultrasound," *Ultrasound Med. Biol.*, vol. 42, no. 9, pp. 2315–2322, Sep. 2016.

YOU-WEI WANG graduated in computer science and information engineering. He received the M.S. degree from National Taipei University, New Taipei City, Taiwan, in 2014. He is currently pursuing the Ph.D. degree with National Taiwan University, Taipei, Taiwan. He is full of enthusiasm about medical image processing and deep learning. He would like to devote himself to these works.

CHUNG-CHIEN LEE graduated from National Taiwan University. He is currently pursuing the M.D. and Ph.D. degrees with the Graduate Institute of Biomedical Electronics and Bioinformatics, National Taiwan University, Taipei, Taiwan. He is also an Orthopedic Surgeon with the Department of Orthopedic Surgery, New Taipei City Hospital, New Taipei City, and the Department of Orthopedic Surgery, National Taiwan University Hospital, Taipei.

CHUNG-MING LO graduated from National Taiwan University. He is currently an Associate Professor with the College of Medical Science and Technology, Taipei Medical University, Graduate Institute of Biomedical Informatics, Taipei, Taiwan. His research interests include medical image processing, deep learning, and multimedia information retrieval.